Research Article Vol. 57, No. 28 / 1 October 2018 / Applied Optics 8467

applied optics

VCSEL mode and polarization control by an elliptic dielectric mode filter

Lei Xiang,[1,2] Xing Zhang,[1,*] JianWei Zhang,[1] YouWen Huang,[1] Werner Hofmann,[3] YongQiang Ning,[1] and LiJun Wang[1]

[1]Changchun Institute of Optics, Fine Mechanics and Physics, Chinese Academy of Sciences, Changchun 130033, China
[2]University of Chinese Academy of Sciences, Beijing 100049, China
[3]Technical University of Berlin, Berlin 10623, Germany
*Corresponding author: zhangx@ciomp.ac.cn

Received 29 May 2018; revised 11 September 2018; accepted 11 September 2018; posted 11 September 2018 (Doc. ID 332700); published 1 October 2018

In this paper, we demonstrate the effectiveness of polarization mode control in vertical-cavity surface-emitting lasers (VCSELs) with integrated elliptic dielectric mode filters. The single-mode single-polarization laser operation is obtained by an irregularly shaped oval dielectric mode filter, aimed at cost-effective mass production. The orthogonal polarization suppression ratio was measured to be 16.7 dB, and the side-mode suppression ratio exceeded 30 dB. A single fundamental mode power of 0.55 mW was achieved at a bias current of 4 mA. We compared the spectra and near-field intensities of the dielectric mode filter VCSEL with a reference device. The comparison clearly indicates the effectiveness of our dielectric mode filter in controlling the transverse- and polarization-mode properties of VCSELs.

OCIS codes: (250.5960) Semiconductor lasers; (250.7260) Vertical cavity surface emitting lasers; (140.3295) Laser beam characterization.

https://doi.org/10.1364/AO.57.008467

1. INTRODUCTION

Vertical cavity surface-emitting lasers (VCSELs) have numerous unique advantages such as single-longitudinal mode output, narrow circular beam, high modulation bandwidth, and manufacturability of monolithic 2D arrays [1–4]. The implementation of single-transverse mode single-polarization lasing has always been an attractive research topic in the field of VCSELs. Moreover, typically stable single-mode and single-polarization VCSELs are desired in communication and sensing applications [5–8]; however, high output power levels are difficult to achieve. Reducing the active volume with small oxide apertures (smaller than 4 μm) is a traditional method to control the transverse mode configurations in VCSELs. This has drawbacks such as low single-mode output power, large differential resistance, and high current density. To solve the conflict between oxide aperture and high-power single-mode output, another method of mode control is needed. The importance of mode control in practical applications is critical, but the various mode control methods are still under investigation. Several methods, such as surface relief [9,10], photonic crystal waveguides [11], wedge-shaped holey structures [12], microlenses [13], Zn diffusion structure [14], and small oxide apertures [15], have been developed in recent years to control the mode characteristics. Some efforts have been utilized to control the polarization stabilization via minimally invasive focused electron beam triggered chemistry [16]. However, the aforementioned methods have disadvantages, such as complex epitaxial growth and device processing, high precision control of etching depth, and limited oxide aperture, which deter their industrial mass production.

In this study, a dielectric mode filter is proposed to resolve the manufacturability issues of large oxide aperture VCSELs with single-mode single-polarization outputs, which are designed to enable their mass production in practical applications. This method is applied to conventional VCSEL production via lithography, and a stable emission in the fundamental mode is achieved. Relative to the traditional mode of control methods, the dielectric mode filter of the VCSEL needs only a single step of SiO_2 deposition and does not need additional lithographic steps. Similarly, by depositing a dielectric material SiO_2 on the surface to achieve current insulation and mode control (i.e., one photolithography and etching step), a spatially dependent out-of-phase configuration without semiconductor etching or regrowth is achieved, thereby suppressing higher-order modes and realizing the mode control [17].

2. DEVICE DESIGN AND FABRICATION

The 850 nm VCSEL wafer is grown by metal-organic chemical vapor deposition. The epitaxial structure consists of an *n*-type

DBR with 34 pairs of $Al_{0.12}Ga_{0.88}As/Al_{0.9}Ga_{0.1}As$, followed by an active region with three strained GaAs quantum wells of 7.2 nm thickness. The cavity around the active region is a one-wavelength-long $Al_{0.3}Ga_{0.7}As$ spacer. The *p*-type DBR with 20.5 pairs of $Al_{0.12}Ga_{0.88}As/Al_{0.9}Ga_{0.1}As$ is followed by a GaAs cladding layer. The current aperture is realized by an $Al_{0.98}Ga_{0.02}As$ layer with a thickness of 30 nm inserted between the active region and the *p*-DBR. The cross-sectional view of the VCSEL structure is shown in Fig. 1. At the output window of the VCSEL, a dielectric mode filter formed by an elliptic SiO_2 layer is deposited on the central region of the device to suppress the higher-order transverse modes and to control polarization. The donut-shaped SiO_2 layer raises the mirror losses of the transverse modes that overlap with the outer area. According to the standard fabrication process, the VCSEL mesa is formed with inductively coupled plasma reactive ion etching. To achieve the current and light confinement, an oxide aperture with a diameter of 6 μm is formed by selectively oxidizing the $Al_{0.98}Ga_{0.02}As$ layer. Then, the SiO_2 protection layer is deposited by plasma-enhanced chemical vapor deposition. The elliptic donut-shaped SiO_2 dielectric mode filter, output window, and contact area are defined simultaneously by the next single photolithographic process, and the SiO_2 layer is etched by inductively coupled plasma reaction ion etching. The short half-axis of the inner mode filter is 1 μm, while the long half-axis is 1.6 μm, the outer radius of elliptic filter (circular) is 4 μm, and the thickness of the SiO_2 is 145 nm. This single photolithographic process will help to reduce manufacturing costs and improve production yield. The *p*- and *n*-contacts are formed at the top and bottom side of the VCSEL structure, respectively. In the experiment, we design a reference device without a mode filter for comparison. The reference device has the same diameter of mesa and oxide aperture on this wafer, and the two types devices have an identical fabrication process.

A refractive index model is established to simulate VCSELs with oxide aperture diameters of 6 μm and determine the transverse mode characteristics of such large VCSEL configurations. When the diameter of the oxide aperture is smaller than 6 μm, the small mode volume and high degree of mode overlap reduces the fundamental mode output power, which subsequently results in the complex suppression of higher-order modes. First, we use COMSOL to simulate the optical field distribution in the active region. The mesa diameter used is 20 μm, and the oxide aperture diameter is 6 μm. To obtain the fundamental mode (LP_{01}), the distribution of the mode along the radius is considered (as shown in Fig. 2). In these figures, LP_{01} is distributed at the center of the waveguide region, LP_{01} and LP_{11} have certain degrees of overlap, and higher-order modes of LP_{11} and LP_{21} are distributed near the edge of the oxide aperture. The dielectric mode filter can be introduced in the higher-order mode regions to tailor the cavity properties. This method can also selectively discriminate the unwanted higher-order modes. An elliptic shape is adopted for the mode filter because it can break the circular symmetry structure and subsequently achieve the single-mode and single-polarization output. We adopt the 1 μm radius of the dielectric mode filter from the simulation, particularly from the intersection of LP_{01} and LP_{11}. The different transverse modes have various degrees of overlap, and LP_{01} will experience relatively higher losses when the radius of the dielectric mode filter is 1 μm. However, this configuration requires an optimization of the elliptic donut-shaped dielectric mode filter. By reducing the size of the mode filter, the threshold current of the fundamental mode can be increased, and the single-mode output power can be decreased simultaneously. Moreover, the diameter of the mode filter is extremely large, a higher-order mode LP_{11} can reach threshold much earlier and lase, which then influences the fundamental mode output power. The mode filter pattern is elliptical in our experiment. Finally, the short half-axis of mode filter is 1 μm and can suppress high-order modes, while the long half-axis is 1.6 μm and can break the circular symmetry.

The reflectivity of the top surface of the VCSEL structure is determined by calculating for different thicknesses of SiO_2 films on a 1D plane-wave transfer matrix. The relationship between the threshold gain and the thickness of the dielectric mode filter (SiO_2 layer) is also established (Fig. 3). The threshold modal gain Γg_{th} can be expressed as [18]

$$\Gamma g_{th} = a_{in} + \frac{1}{L}\ln\frac{1}{\sqrt{R_t R_d}}, \tag{1}$$

where Γ is the optical confinement factor, g_{th} is threshold material gain, a_{in} is intrinsic internal loss, and R_t and R_d represent the reflectivity of the top and bottom of the distributed

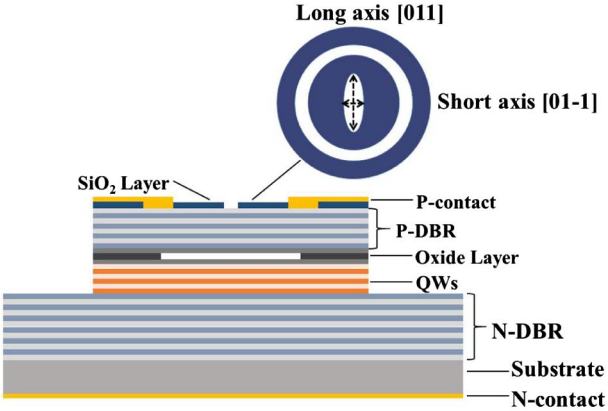

Fig. 1. Cross-sectional view of elliptic donut-shaped SiO_2 VCSEL.

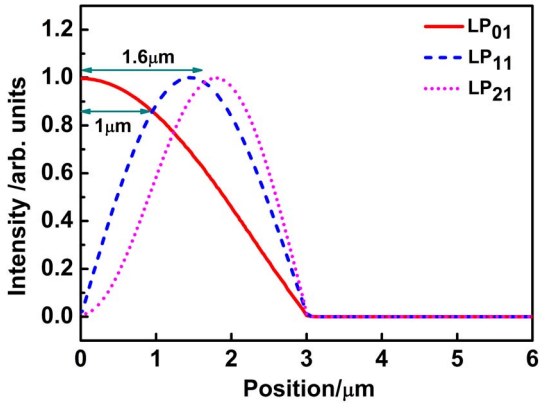

Fig. 2. Distribution of the LP_{01}, LP_{11}, and LP_{21} modes along the radius direction.

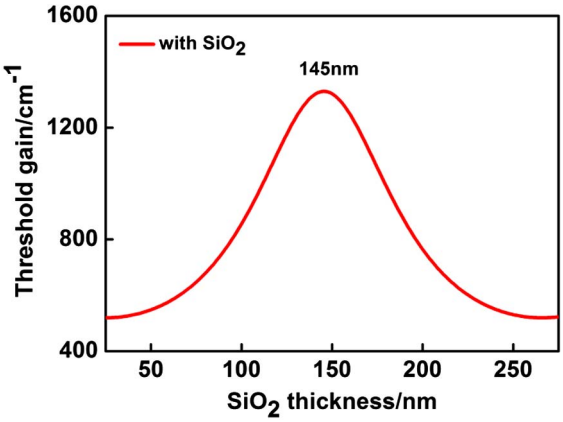

Fig. 3. Simulation of 6 μm oxide-confined VCSEL: Relationship between threshold modal gain and SiO_2 thickness.

Bragg reflectors (DBRs). Threshold modal gain Γg_{th}, which is the product of the optical confinement factor, and the threshold material gain is determined by the layer thickness and refractive index of the SiO_2 film in this experiment. Γg_{th} will elevate because of the decrease in the mirror reflectivity of the SiO_2 film (i.e., R_t and R_d). Furthermore, Γg_{th} is proportional to mirror loss. To implement the selective mode control, the mode filter should minimize the threshold modal gain at the center of top surface and maximize it in the higher-order mode region. From the simulation, the threshold modal gain can reach the maximum 145 nm thickness of the SiO_2 layer. At this point, the device has the maximum threshold modal gain with the highest mirror loss. By spatially controlling the SiO_2 deposition as a dielectric mode filter, we can reserve the SiO_2 layer on top of the higher-order mode region to selectively discriminate these higher-order modes and etch off the SiO_2 layer to realize a low-loss region at the center of the top surface. Therefore, the transverse modes can be selectively suppressed. An elliptic donut-shaped area for the mode control can be formed by dielectric mode filtering.

3. RESULTS AND DISCUSSION

Figure 4 shows the lasing characteristics of the VCSEL with an elliptic donut-shaped SiO_2 mode filter and the conventional reference device measured in continuous wave operation at room temperature. Both structures (with/without mode filter) come from the same epitaxial wafer, and they have the same oxide aperture size because of the identical fabrication process. The output power is also measured polarization dependent with a polarizer along the [011] and [01-1] crystal orientations of the epitaxial wafer. A comparison between the two devices shows that the reference VCSEL has poor polarization characteristics given that polarization switches and mode-hops will occur within the normal operation regime. The VCSEL with our novel mode-filter, however, shows single-mode single-polarization operation with the power along the [011] orientation being much greater than along the [01-1] direction. The single fundamental mode power reaches 0.55 mW at a driving current of 4 mA. The side-mode suppression ratio exceeds 30 dB, and the maximum orthogonal polarization suppression

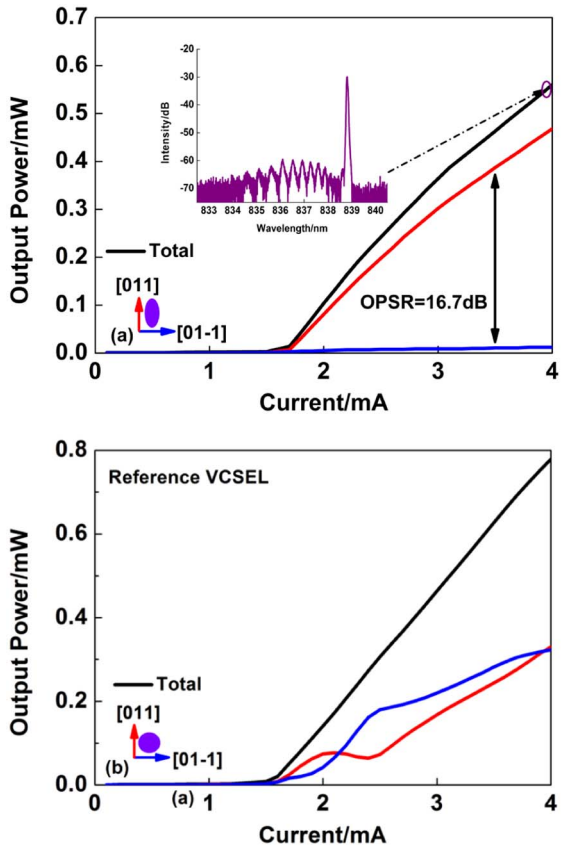

Fig. 4. Output power–current characteristics of VCSEL. (a) Elliptic device. (b) Reference device.

ratio is measured to be 16.7 dB, which shows that the elliptic geometry of our SiO_2 mode-filter has a significant effect on mode and polarization control. Only the two crystal orientations of [011] and [01-1] are considered because of the gain material properties and practical results, indicating that polarization pinning can only be achieved along the major crystal orientations by means of elliptical surface etching [19]. The direction of the elliptical etching along [011] and [01-1] is adopted in this experiment, in which [011] is the long axis and [01-1] is the short axis. Our mode filter can effectively break the circular symmetry, and the electro-optic effect will induce this anisotropy, which is related to the electrical field. Meanwhile, the birefringence and dichroism between the modes are induced by the Pockels effect, which has an important influence on polarization in accordance with modal frequency and threshold gain differences, respectively [20,21]. However, related results have been reported in the literature. Researchers have proven that the Pockels effect slightly prefers [01-1] polarization, but the weak effect is insufficient in changing integral polarization characteristics. TE and TM vary in terms of reflection along the different directions of the elliptical axis, and polarization will preferentially select the polarization with high effective reflection coefficient, i.e., the long axis direction [011] [22], which has an important influence on the integral polarization characteristics. In summary, the polarization selection is introduced by the anisotropic elliptically etched SiO_2 layer.

The spectra of elliptic donut-shaped SiO_2 and the conventional VCSEL are tested under $I = 3$ mA at room temperature (Fig. 5). The blue line represents the spectra of the conventional VCSELs. Multimode operation due to large aperture size can be observed, and the situation implies numerous complicated modes that contribute to the lasing action when the current is 3 mA. The mode-filtered VCSELs operate in a stable single-mode regime, and higher-order modes are well suppressed. The comparative result between the elliptic donut-shaped SiO_2 and the conventional VCSEL suggests that the former has a specific impact on optical properties. The mode filter increases the threshold modal gain of the higher-order modes, thereby suppressing the lasing. To understand the mode differences between elliptic donut-shaped SiO_2 and conventional VCSEL, the near-field characteristics are measured at the current of 3 mA, as shown in Figs. 6(a) and 6(b). Coincident with the spectra, only the single-transverse mode pattern can be seen from the elliptic donut-shaped SiO_2 VCSEL, and the higher-order modes are well suppressed at this operation range. By contrast, the conventional device has two deep-colored regions that represent lasing of higher-order modes. On the basis of this comparison, the elliptic donut-shaped SiO_2 can serve as the dielectric mode filter and suppress the higher-order modes. Therefore, the novel method of the mode control is realized.

The theoretical calculation of transverse mode wavelength can be expressed as [23]

$$\lambda_{\mathrm{LP}} = \lambda_B \left[1 - (2p + l - 1)\lambda_B \frac{\sqrt{n_0 - n_c}}{\sqrt{2}\pi\sqrt{n_0 n_0 a}}\right], \qquad (2)$$

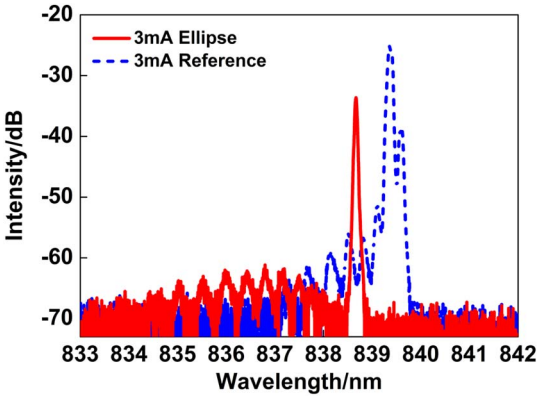

Fig. 5. Output spectrum of the VCSEL. (red) Elliptic device. (blue) Reference device.

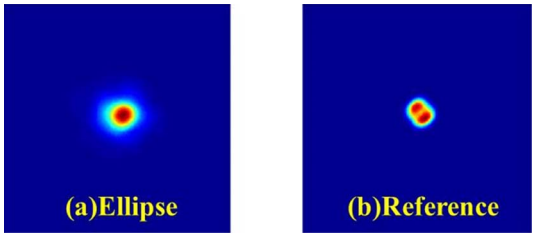

Fig. 6. Near-field pattern of the VCSEL. (a) Elliptic device. (b) Reference device.

where λ_{LP} and λ_B represent the LP mode wavelength and the Bragg wavelength, respectively; l and p represent the azimuthal and radial mode orders; a is the radius of the oxide aperture; and n_0 and n_c are the refractive index of the core layer and cladding layer, respectively. The wavelength of different modes in the elliptic donut-shaped SiO_2 VCSEL is shown in Fig. 7. The higher-order modes have shorter wavelengths than that those of the fundamental mode, and the LP_{11} mode is the next mode to reach threshold and lase [24]. The wavelength spacing between the LP_{01} mode and LP_{11} mode is calculated, $\Delta\lambda = 0.6$ nm, and the experimental and theoretical results are basically consistent. To fully comprehend the dynamic changes of the mode behavior, the spectra of the elliptic donut-shaped SiO_2 VCSEL are measured with varying currents (Fig. 8). The number of modes notably decreased because of the mode filter effect. The elliptic donut-shaped SiO_2 VCSEL has a threshold current of 1.7 mA, and the fundamental mode continued until 4.5 mA, at which the higher-order mode (LP_{11}) appears. The fundamental mode (LP_{01}) reached the threshold first because the LP_{01} mode experienced a smaller cavity loss compared with the other modes. The threshold of LP_{11} mode stayed at 4.5 mA, and this LP_{11} mode behavior is caused by spatial hole burning because the LP_{01} mode depleted the carriers via stimulated recombination. Therefore, the competition between the LP_{01} and LP_{11} mode is realized when the current

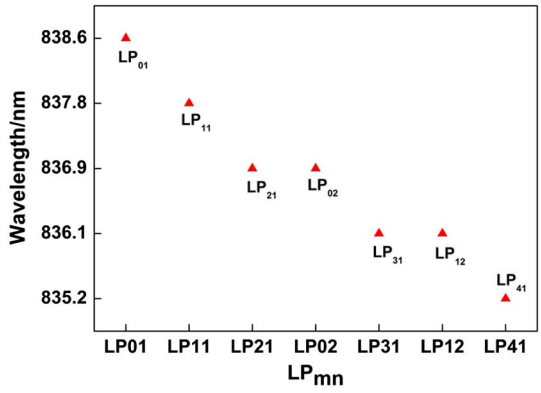

Fig. 7. Calculated wavelengths of different modes in elliptic donut-shaped SiO_2 VCSEL.

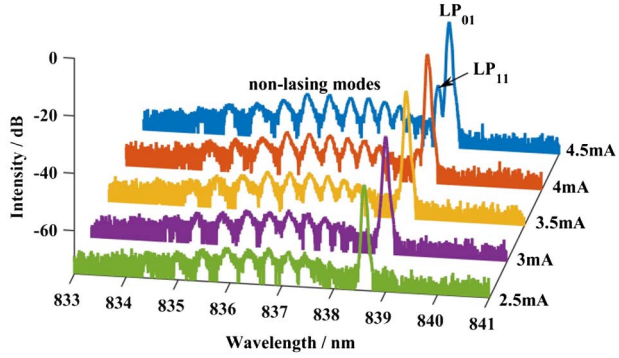

Fig. 8. Spectra of the elliptic donut-shaped SiO_2 VCSEL under varying currents.

exceeds 4.5 mA. The near-field intensity of the LP_{11} mode can be expressed as [25]

$$S_{lp}(r,\phi) \propto \left\{ \begin{matrix} \cos^2(l\phi) \\ \sin^2(l\phi) \end{matrix} \right\} \exp\left(-\frac{2r^2}{w_0^2}\right), \quad (3)$$

where (r,ϕ) are cylindrical coordinates; l and p represent the azimuthal and radial mode orders, respectively; and w_0 is the mode field radius. The $\cos^2(l\phi)$ and $\sin^2(l\phi)$ terms provide the LP_{11} mode with strong waveguide action and photon–carrier interaction. The shorter wavelength of the LP_{11} mode is the next lasing mode after the LP_{01} mode. Some nonlasing modes can be observed in the spectrum, and they are induced by the spontaneous emission of individual modes. These nonlasing modes will dominate when the current is less than the threshold, and they will be clamped when the current is above the threshold. A redshifting of the overall spectrum occurs when the current is increased (a scenario caused by pronounced heating). In summary, the mode filter is effective and can modify the optical properties of VCSELs.

4. CONCLUSION

We simulated and experimentally verified the influence of the elliptic donut-shaped SiO_2 layer on the transverse mode behavior of VCSELs, and the method is realized with mode control by using the dielectric mode filter. The 6 μm oxide aperture of the 850 nm elliptic donut-shaped SiO_2 VCSEL is designed and demonstrated, and reproducing the single-fundamental-mode VCSEL with stable emission can be realized. Here, we present a novel method to achieve mode control of VCSELs with large oxide apertures that feature superior optical device properties. This method has a simple design and can be easily generalized to other types of devices. This method is used to realize high-power single-mode devices by further optimizing the parameters of the oxide aperture and the dielectric mode filter.

Funding. National Key Research and Development Project (2016YFE0126800); National Natural Science Foundation of China (NSFC) (61434005, 61474118, 11774343, 11674314); Science and Technology Program Jilin Province (20160203013GX); Youth Innovation Promotion Association (2017260); Jilin Province Science and Technology Development Project (20160204073GX).

REFERENCES

1. T. Siegle, S. Schierle, S. Kraemmer, B. Richter, S. F. Wondimu, P. Schuch, C. Koos, and H. Kalt, "Photonic molecules with a tunable inter-cavity gap," Light Sci. Appl. **6**, e16224 (2017).
2. J. W. Zhang, X. Zhang, H. B. Zhu, Y. Q. Ning, L. Qin, and L. J. Wang, "High-temperature operating 894.6 nm-VCSELs with extremely low threshold for Cs-based chip scale atomic clocks," Opt. Express **23**, 14763–14773 (2015).
3. Y. Mei, G. E. Weng, B. P. Zhang, J. P. Liu, W. Hofmann, L. Y. Ying, J. Y. Zhang, Z. C. Li, H. Yang, and H. C. Kuo, "Quantum dot vertical-cavity surface-emitting lasers covering the green gap," Light Sci. Appl. **6**, e16199 (2017).
4. H. Q. Wang, T. P. Zhao, J. Xu, D. Y. He, L. Lv, H. Q. Gui, W. Huang, H. Ming, and J. P. Xie, "Optimized design of laser range finding system using the self-mixing effect in a single-mode VCSEL," Chin. Opt. Lett. **4**, 87–90 (2006).
5. K. K. Huang, N. Li, and X. H. Lu, "A High sensitivity laser-pumped cesium magnetometer," Chin. Phys. Lett. **29**, 100701 (2012).
6. S. Knappe, V. Shah, P. D. D. Schwindt, L. Hollberg, J. Kitching, L. A. Liew, and J. Moreland, "A microfabricated atomic clock," Appl. Phys. Lett. **85**, 1460–1462 (2004).
7. A. Alsamaneh, M. B. Sanayeh, M. J. Miah, W. Schwarz, D. Wahl, A. Kern, and R. Michalzik, "Polarization-stable vertical-cavity surface-emitting lasers with inverted grating relief for use in microscale atomic clocks," Appl. Phys. Lett. **101**, 171104 (2012).
8. L. Li, J. C. Zhong, Y. M. Zhang, W. Su, C. L. Yan, Y. Q. Hao, and X. G. Jiang, "Oxide-apertured VCSEL with short period superlattice," Chin. Opt. Lett. **2**, 713–714 (2004).
9. A. Haglund, J. S. Gustavsson, P. Modh, and A. Larsson, "Dynamic mode stability analysis of surface relief VCSELs under strong RF modulation," IEEE Photon. Technol. Lett. **17**, 1602–1604 (2005).
10. A. Haglund, J. S. Gustavsson, J. Vukusic, P. Modh, and A. Larsson, "Single fundamental-mode output power exceeding 6 mW from VCSELs with a shallow surface relief," IEEE Photon. Technol. Lett. **16**, 368–370 (2004).
11. A. J. Danner, T. S. Kim, and K. D. Choquette, "Single fundamental mode photonic crystal vertical cavity laser with improved output power," Electron. Lett. **41**, 325–326 (2005).
12. A. Furukawa, S. Sasaki, M. Hoshi, A. Matsuzono, K. Moritoh, and T. Baba, "High-power single-mode vertical-cavity surface-emitting lasers with triangular holey structure," Appl. Phys. Lett. **85**, 5161–5163 (2004).
13. Y. W. Huang, X. Zhang, J. W. Zhang, Y. Y. Xie, W. Hofmann, Y. Q. Ning, and L. J. Wang, "Monolithic microlens VCSELs with high beam quality," IEEE Photon. J. **9**, 1–8 (2017).
14. J. W. Shi, C. C. Chen, Y. S. Wu, S. H. Guol, C. H. Kuo, and Y. J. Yang, "High-power and high-speed Zn-diffusion single fundamental-mode vertical-cavity surface-emitting lasers at 850-nm wavelength," IEEE Photon. Technol. Lett. **20**, 1121–1123 (2008).
15. R. Henning, R. Arun, and S. Gunther, "Development of InGaAsN-based 1.3 μm VCSELs," Semicond. Sci. Technol. **17**, 892–897 (2002).
16. I. Utke, M. G. Jenke, C. Röling, P. H. Thiesen, V. Iakovlev, A. Sirbu, A. Mereuta, A. Caliman, and E. Kapon, "Polarisation stabilisation of vertical cavity surface emitting lasers by minimally invasive focused electron beam triggered chemistry," Nanoscale **3**, 2718–2722 (2011).
17. B. Kesler, T. O'Brien, G. L. Su, and J. M. Dallesasse, "Facilitating single-transverse-mode lasing in VCSELs via patterned dielectric anti-phase filters," IEEE Photon. Technol. Lett. **28**, 1497–1500 (2016).
18. X. Zhang, Y. Zhang, J. W. Zhang, J. Zhang, C. Y. Zhong, Y. Q. Ning, S. H. Gu, and L. J. Wang, "894 nm high temperature operating vertical-cavity surface-emitting laser and its application in Cs chip-scale atomic-clock system," Acta Phys. Sinica **65**, 134204 (2016).
19. H. J. Unold, M. C. Riedl, R. Michalzik, and K. J. Ebeling, "Polarisation control in VCSELs by elliptic surface etching," Electron. Lett. **38**, 77–78 (2002).
20. P. Debernardi, G. P. Bava, C. Degen, and I. Fischer, "Influence of anisotropies on transverse modes in oxide-confined VCSELs," IEEE J. Quantum Electron. **38**, 73–84 (2002).
21. M. P. Van Exter, A. K. J. van Doorn, and J. P. Woerdman, "Electro-optic effect and birefringence in semiconductor vertical-cavity lasers," Phys. Rev. A **56**, 845–853 (1997).
22. P. Debernardi, H. J. Unold, J. Maehnss, and R. Michalzik, "Single-mode, single-polarization VCSELs via elliptical surface etching: experiments and theory," IEEE J. Sel. Top. Quantum Electron. **9**, 1394–1405 (2003).
23. Y. M. Su, L. J. Yu, X. Guo, X. Zhang, J. G. Liu, and N. H. Zhu, "Few-mode vertical-cavity surface-emitting lasers for space-division multiplexing," J. Semicond. **38**, 094002 (2017).
24. J. A. Vukusic, H. Martinsson, J. S. Gustavsson, and A. Larsson, "Numerical optimization of the single fundamental mode output from a surface modified vertical-cavity surface-emitting laser," IEEE J. Quantum Electron. **37**, 108–117 (2001).
25. R. Michalzik, *VCSEL Fundamentals* (Springer, 2013).